ADVANCED FUNCTIONAL MATERIALS
www.afm-journal.de

Materials Views
www.MaterialsViews.com

Electronic Structure of Self-Assembled Monolayers on Au(111) Surfaces: The Impact of Backbone Polarizability

By *LinJun Wang, Gerold M. Rangger, Lorenz Romaner, Georg Heimel, Tomas Bučko, ZhongYun Ma, QiKai Li, Zhigang Shuai,** and *Egbert Zojer**

Modifying metal electrodes with self-assembled monolayers (SAMs) has promising applications in organic and molecular electronics. The two key electronic parameters are the modification of the electrode work function because of SAM adsorption and the alignment of the SAM conducting states relative to the metal Fermi level. Through a comprehensive density-functional-theory study on a series of organic thiols self-assembled on Au(111), relationships between the electronic structure of the individual molecules (especially the backbone polarizability and its response to donor/acceptor substitutions) and the properties of the corresponding SAMs are described. The molecular backbone is found to significantly impacts the level alignment; for molecules with small ionization potentials, even Fermi-level pinning is observed. Nevertheless, independent of the backbone, polar head-group substitutions have no effect on the level alignment. For the work-function modification, the larger molecular dipole moments achieved when attaching donor/acceptor substituents to more polarizable backbones are largely compensated by increased depolarization in the SAMs. The main impact of the backbone on the work-function modification thus arises from its influence on the molecular orientation on the surface. This study provides a solid theoretical basis for the fundamental understanding of SAMs and significantly advances the understanding of structure–property relationships needed for the future development of functional organic interfaces.

1. Introduction

Contacts between organic semiconductors and metals decisively determine the charge-carrier injection efficiencies in organic (opto)electronic devices.[1–4] In order to improve charge injection, several surface treatments have been reported.[5–13] One of the most attractive and promising ways is to modify the metal electrodes using self-assembled monolayers (SAMs).[8–12] Here, the SAM is sandwiched between the metal electrode and the active organic material and, thus, allows the effective work function of the electrode to be changed. This enables control of the charge-injection barriers between the electrode Fermi level (E_F) and the frontier electronic states in the organic semiconductor.[9] However, it also introduces an additional tunneling resistance that is determined by the alignment of the electronic states *within* the SAM relative to E_F. The latter also plays a decisive role in molecular electronics, where the SAM itself becomes the active component of the device.[14–20] Consequently, the induced electrode work-function modification and the alignment of the SAM states relative to the metal Fermi

[*] Prof. Z. G. Shuai, L. J. Wang, Z. Y. Ma, Prof. Q. K. Li
Key Laboratory of Organic Solids
Beijing National Laboratory for Molecular Sciences (BNLMS), Institute of Chemistry
Chinese Academy of Sciences
100190 Beijing (P.R. China)
E-mail: zgshuai@tsinghua.edu.cn
Prof. Z. G. Shuai
Department of Chemistry
Tsinghua University
100084 Beijing (P.R. China)
Prof. E. Zojer, G. M. Rangger, Dr. L. Romaner
Institute of Solid State Physics
Graz University of Technology
Petersgasse 16, A-8010 Graz (Austria)
E-mail: egbert.zojer@tugraz.at
Dr. L. Romaner
Department of Material Physics
University of Leoben
Franz-Josef Str. 18/II, A-8700 Leoben (Austria)
Dr. G. Heimel
Insitut für Physik
Humboldt-Universität zu Berlin
Newtonstr. 15, 12489 Berlin (Germany)
Dr. T. Bučko
Fakultät für Physik and Center for Computational Materials Science
Universität Wien
Sensengasse, 1090 Wien (Austria)

DOI: 10.1002/adfm.200901152

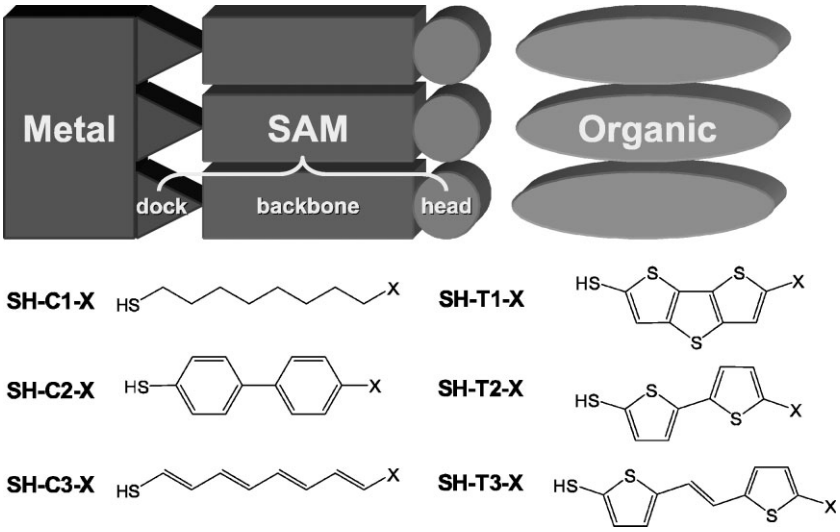

Figure 1. Top: Schematic of a SAM-modified interface between a metal and an organic semiconductor. The SAM consists of three parts: the docking group, backbone, and head group. Bottom: Chemical structures of the molecules studied as SAMs on Au(111). X denotes the head group substituents, -NH_2 and -CN. Accordingly, when only referring to the backbones, the abbreviations **C1**, **C2**, **C3**, **T1**, **T2**, and **T3** are used. The substituted molecules are denoted as backbone-substituent, the thiols as SH-backbone-substituent, and the molecules forming the SAM as S-backbone-substituent.

level constitute the two most important electronic quantities of SAMs in the context of organic and molecular electronics. Only a complete understanding of all factors determining these parameters will allow a systematic improvement of device performance.

The three main components of a SAM, which can be altered to tune its electronic properties, are the docking group, the backbone, and the head group (see Figure 1, top). We have discussed before how head-group substitutions and the choice of the docking group can be used to independently tune the work-function modification and level alignment.[21] Here, we provide a comprehensive theoretical study illuminating the impact of the chemical nature of the backbone. Particular emphasis is laid also on the response of different backbone structures to head-group substitution with either electron-rich (donor) or electron-poor (acceptor) groups. This is not only of practical relevance, but also crucial for obtaining a fundamental understanding of the electronic properties of SAMs: it has been recently shown for biphenyl-thiol SAMs on Au(111)[22] and Ag(111)[23] that such head-group substitutions,[24] as expected, have a significant impact on the effective work function of the SAM-covered substrate. However, in spite of the fact that substitutions result in significant changes in the molecular ionization potentials (*IP*s) and electron affinities (*EA*s), no effect on the alignment between the molecular bands and the metal Fermi level (E_F) has been observed in close-packed SAMs. In other words, head-group substitution in those systems does not affect the electronic structure in the immediate vicinity of the metal/SAM contact.[22,25]

Two approaches can be envisioned to avoid this effect: i) If the decoupling were merely a consequence of the aromatic character of the biphenyl backbone making it little susceptible to rearrange its electron cloud in response to donor or acceptor substitutions, it might prevent the head groups from ''communicating'' through the SAM with the metal/docking-group contact. This could be avoided by employing SAMs of molecules with a non-aromatic but fully π-conjugated backbone, where substitution with π-donors or -acceptors can be expected to have a more pronounced effect. ii) When investigating the packing-density dependence of the electronic structure of SAMs,[26,27] Romaner et al.[28,29] observed a significant depolarization of dipolar molecules in monolayers induced by the dipole moments of neighboring molecules. If such a ''screening'' of the substituents by the backbone were responsible for the lack of changes in level alignment upon donor/acceptor head-group substitution, the situation should change in SAMs of molecules with less polarizable, nonconjugated backbones.

Thus, to elucidate the role of the backbone of SAM-forming molecules, we employed slab-type band-structure calculations[30] based on density functional theory (DFT) on a systematic series of molecules self-assembled on Au(111). We specifically focused on a) whether the chemical nature and the polarizability of the backbone qualitatively changes the impact of donor/acceptor head-group substitutions on the level alignment, b) how the backbone itself impacts the level alignment, and c) to what extent the choice of the backbone affects the SAM-induced work-function modification. First, the properties of the isolated backbones are described in some detail, as they are the key ''input parameters'' for the present study. After discussing important issues regarding the structure of the various SAMs, we turn to the level alignment, analyze trends in the work-function modification, and finally, address the impact of the SAM packing density.

2. Description of the Investigated Systems

2.1. The Molecules

The investigated molecules are depicted in the bottom part of Figure 1 (see figure caption for naming conventions). For each backbone, we considered a donor- ($X = -NH_2$) and an acceptor- ($X = -CN$) substituted version. In addition to the aromatic biphenyl backbone (**C2**) as the reference system,[21–23,25,28–33] we studied a nonconjugated alkane (**C1**) and a fully π-conjugated alkene (**C3**). Additionally, thiophene-based molecules (**T1**, **T2**, and **T3**) were considered as intrinsically more electron-rich, fully conjugated, but non-aromatic backbones. With the exception of **T3**, the lengths of all backbones are comparable.

The molecular properties of these backbones, which are key to understanding the interface energetics in the respective SAMs,[34,35] are summarized in Table 1. Unless otherwise noted, the values refer to the backbones alone, that is, without head and docking groups. As expected, the electronic polarizability along the long molecular axes, α_{zz}, is largest for **C3** and **T3**. Especially the latter is, thus, a good example for enhanced polarizability through increased conjugation length (extra vinylene unit). In **C1**, α_{zz} is

Table 1. Molecular electronic properties of all investigated backbones. Values are reported for the unsubstituted backbones bearing neither substituent nor an -SH docking group. Exceptions are $\Delta E_{H\text{-}NH2}$ and $\Delta E_{H\text{-}CN}$, where $-NH_2/-CN$ substituents were added. *IP* (*EA*) are the vertical ionization potentials (electron affinities) [a]. E_{HOMO} is the energy of the highest occupied molecular orbital for the unsubstituted backbone, α_{zz} is the *zz* component of the polarizability tensor, with *z* being the long molecular axis defined as connecting the two terminal C atoms. $\Delta E_{H\text{-}NH2}$ ($\Delta E_{H\text{-}CN}$) is the change of the HOMO energy upon substitution with an $-NH_2$ ($-CN$) head group [b]. μ_{CN} (μ_{NH2}) is the total dipole moment of the CN$-$ (NH_2-) substituted molecule and φ_{CN} and φ_{NH2} are the respective angles between the dipole moments and the long molecular axes. All dipole moments are given in Debye (D); a positive sign refers to the dipole moment pointing from the backbone towards the substituent. Additional molecular parameters can be found in Table S1 in the Supporting Information.

Backbone	*IP* [eV]	*EA* [eV]	Hardness [eV]	E_{HOMO} [eV]	α_{zz} [Bohr^3]	$\Delta E_{H\text{-}CN}$ [eV]	$\Delta E_{H\text{-}NH2}$ [eV]	μ_{CN} [D]	φ_{CN} [°]	μ_{NH2} [D]	φ_{NH2} [°]
C1	9.45	−3.66	6.56	−6.99	115	−0.29	2.00(–0.05)	−4.28	32	1.30[c]	35
C2	7.61	−0.56	4.09	−5.30	211	−0.49	0.83	−5.33	0	2.60	23
C3	7.11	0.04	3.53	−4.76	288	−0.54	0.82	−6.02	18	4.58	12
T1	7.30	−0.49	3.90	−4.93	198	−0.55	0.66	−5.69[d]	16	2.51[d]	27
T2	7.21	−0.39	3.80	−4.80	192	−0.57	0.66	−5.52	12	2.57	25
T3	6.74	0.15	3.30	−4.57	327	−0.51	0.55	−6.23	9	3.17	20

[a] Electron affinities are defined here as the total energy of the neutral system minus that of the negatively charged molecule. [b] Defined as the energy of the HOMO of the substituted system minus the energy of the HOMO of the unsubstituted system. [c] In the single-molecule optimizations of **C1**$-NH_2$ a lower energy conformer with a dipole moment of 1.44 D is found; there, the plane of the $-NH_2$ group is perpendicular to the plane of the backbone. This prevents an efficient mixing of the nitrogen lone pair with backbone states so that the $-NH_2$ group largely loses its donating character. This molecular conformation is, however, found to be unfavorable on the surface, where a structure with the -NH_2 plane close to coplanar with the backbone is found; therefore, we report here the molecular dipole moment for such a situation. [d] The fact that the **T1** backbone is noncentrosymmetric has only a minor impact on the total dipole moment as can be inferred from the unsubstituted molecule having a dipole moment of only 0.48 D.

smaller by a factor of more than 2.5 and **C2**, **T1**, and **T2** display intermediate values. A suitable parameter to characterize the potential impact of chemical substitution is the *chemical hardness* of a molecule.[36] It is a measure for the ability of a molecule to resist changes of its electron cloud and is defined as half the difference between *IP* and *EA*.[37] As can be seen in Table 1, the chosen backbones span a wide range of chemical hardness. For example, for **C1** it is nearly twice as large as for **T3** and **C3**; **C2** has the second largest hardness of the backbones in spite of its polarizability being slightly larger than that of **T1** and **T2**.

The impact of the substitution on the molecules' energy levels can be estimated by comparing the highest occupied molecular orbital (HOMO) energies of the bare backbones with those of the CN- and NH_2-substituted ones. Substitution with the π-accepting -CN group results in a stabilization of the occupied orbitals by up to −0.57 eV (for **T2**); only for **C1**, which contains no π-electrons, the effect is significantly smaller. Interestingly, for **T3** the change is only −0.51 eV in spite of the fact that this molecule has the highest long-axis polarizability (and the lowest chemical hardness). This hints towards the fact that it is not the ''overall'' polarizability of the backbone, expressed by α_{zz}, which matters for the substitution effect. The relevant quantity is rather the ''local polarizability'' in the region of the molecule where the substituent is attached. Substitution with the π-donor $-NH_2$ results in a destabilization of the HOMOs, which is smaller for the thiophene-based systems as a consequence of the already electron-rich character of these backbones. What appears surprising at first glance is the very large destabilization of the HOMO by nearly 2 eV in the NH_2-substituted alkane **C1**. A closer inspection, however, reveals that this is simply a consequence of the HOMO in **C1**-NH_2 being localized on the substituent. As such, it does not constitute a continuous transport channel through the SAM. In fact, the highest lying delocalized state (of σ-character) in **C1** is almost unchanged upon NH_2-substitution; its position is given in parentheses in Table 1.

The parameters most apparently influencing the magnitude of the SAM-induced work-function modification are the molecular dipole moments, μ_{CN} and μ_{NH2}. For the $-CN$ and $-NH_2$ substituents, the dipoles point in opposite directions; moreover, the absolute values of the dipole moments of the CN-substituted molecules are significantly larger. The dipole moments are largest for the two most polarizable and least chemically hard backbones **C3** and **T3** and smallest for the least polarizable and chemically hardest backbone **C1**. This implies that—in addition to the intrinsic dipole moments of the substituents—a certain amount of charge is transferred to/from the backbone, which is more pronounced for the more polarizable, less chemically hard backbones (an aspect that has to be considered when later discussing depolarization effects). A charge transfer between substituent and backbone is also consistent with the electron-rich thiophene-based backbones having particularly large dipole moments when substituted with an acceptor.

In this context, however, it must be stressed that, apart from **C2**-CN, the dipole axes are not parallel to the long molecular axes (see values of φ_{CN} and φ_{NH2} in Table 1). The main reason for the variations in the dipole orientations is that, for all backbones apart from **C2**, the substituents point in directions different from the long molecular axes. As expected from the structure of the molecules sketched in Figure 1, this effect is most pronounced in **C1** ($\varphi_{CN,C1} = 32°$) and **C3** ($\varphi_{CN,C3} = 18°$); the reason for the smaller value in **C3**-CN is that the dipole is also in part located on the backbone as a result of head-group/backbone charge transfer (see above). The overall situation is slightly more complex for -NH_2, where an out-of-plane component of the dipole moment also exists, as the $-NH_2$ group is not exactly coplanar with the backbone (i.e., it adopts a slightly pyramidal structure).

2.2. Structure of the SAMs on the Surface

As a next step, details of the calculated adsorption geometries need to be discussed. In the present study, all molecules are supposed to

adsorb on the metal upon hydrogen removal from the thiol docking group.[22] For reasons of consistency, the same $p(\sqrt{3} \times 3)$ surface unit cell containing two molecules has been assumed for all SAMs. There, the surface area per molecule is consistent with that found for alkane thiols (**C1**) on Au(111).[38,39] Moreover, biphenylthiols are known to assemble in this unit cell on Au(111) in the characteristic herringbone pattern shown for S-**C2**-CN in Figure 2a.[40]

To model an infinitely extended 2D-periodic surface, the repeated-slab approach was employed with five layers of gold atoms representing the Au(111) surface (see Experimental Section for further details). For the geometry optimizations, a recently developed scheme relying on internal coordinates was used[41] in order to obtain reasonable estimates for the tilt angles of the long molecular axes relative to the surface normal. This proved necessary because with common optimizers relying on Cartesian coordinates very different optimum structures are obtained.[42] These are all higher in energy even when enforcing very tight convergence criteria. The main deviations are found for the tilt angles of the molecular axes with respect to the surface normal, γ, because they correspond to extremely soft degrees of freedom.[43] Importantly, variations in γ have an immediate consequence for the directions of the molecular dipole moments, as shown for the examples of S-**C1**-CN, S-**C2**-CN, and S-**C3**-CN in Figure 2c, d, and e, respectively.

We note that even with internal coordinate optimization a number of different local-minimum structures are found that are very close in energy (within 0.16 eV; see Supporting Information). For example, in the NH_2-substituted systems different conformations exist with different orientations of the slightly pyramidal substituent. Moreover, for the most loosely packed system (**C3** backbone with the less bulky -CN substituent, S-**C3**-CN) we find a layered conformation of the backbones (Fig. 2b) to be energetically preferable over the herringbone structure (Fig. 2a). In the following, results obtained for the lowest-energy conformations will be reported; results for other local-minimum conformations can be found in the Supporting Information. However, one should keep in mind that, at room temperature, it cannot be excluded that domains exist in which other low-energy structures are present; a complete scanning of the highly complex potential energy surfaces for all investigated systems is beyond present computational possibilities.

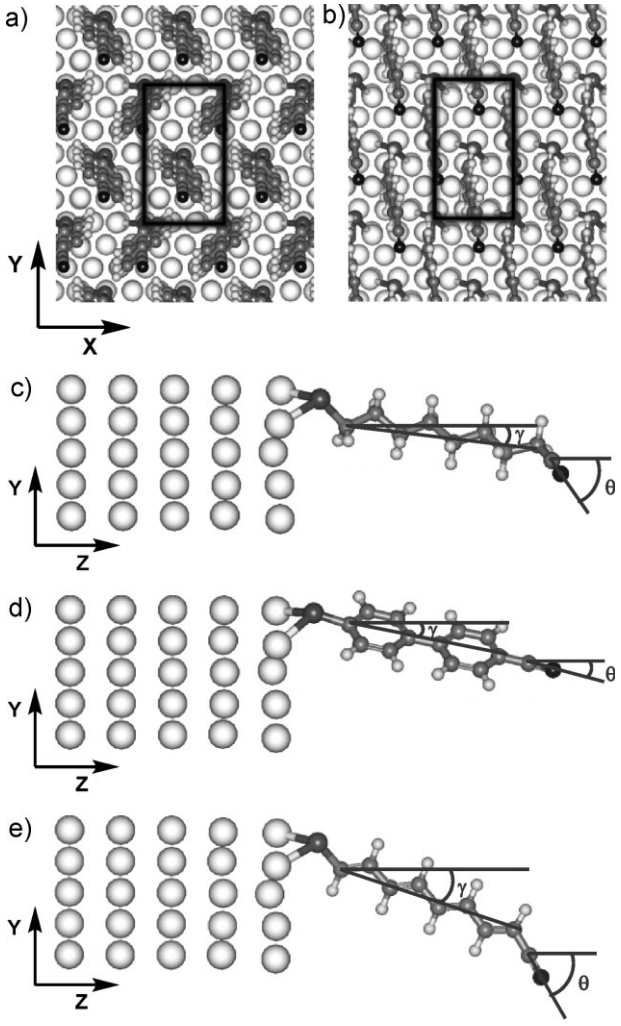

Figure 2. a) Top view of S-**C2**-CN on Au(111). Two molecules per $p(\sqrt{3} \times 3)$ unit cell are arranged in a herringbone pattern. b) Layered conformation identified as the lowest-energy structure for S-**C3**-CN. c–e) Side views of S-**C1**-CN, S-**C2**-CN, and S-**C3**-CN on Au(111). Only one molecule is shown for the sake of clarity. The long molecular axes (γ) and the substituent axes (θ) are titled relative to the surface normal.

3. Electronic Structure of SAMs Bonded to the Au(111) Surface

3.1. Level Alignment

To introduce all relevant quantities and to illustrate their interrelation, the plane-averaged electron potential energy for a SAM of S-**C3**-NH_2 bonded to the five-layer gold slab is shown as an example in the left panel of Figure 3. E_F is the Fermi energy of the

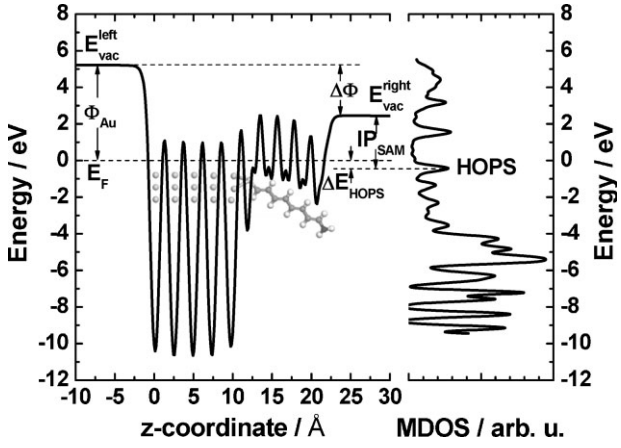

Figure 3. Left: Plane-averaged electron potential energy across a SAM of S-**C3**-NH_2 on a 5-layer Au(111) slab. Right: Corresponding density of states projected onto the molecular layer, MDOS. The origin of the energy axis is the Fermi level (E_F). Also indicated are the left and right vacuum levels (E_{vac}^{left}, E_{vac}^{right}), the gold work function ($\Phi_{Au} = E_{vac}^{left} - E_F$), the work-function modification ($\Delta\Phi = E_{vac}^{right} - E_{vac}^{left}$), the highest occupied π-states (HOPS), the energy position of the HOPS with respect to E_F ($\Delta E_{HOPS} = HOPS - E_F$), and the ionization potential of the SAM ($IP_{SAM} = E_{vac}^{right} - HOPS$).

Table 2. Electronic properties of the various donor- and acceptor-substituted SAMs on Au(111). ΔE_{HOPS} refers to the alignment of the highest occupied states delocalized over the backbone (HOPS) and the metal Fermi level; IP_{SAM} is the ionization potential of the SAM defined as the energetic difference between the HOPS peak and the vacuum level; $\Delta\Phi$ is the SAM-induced work-function modification; the angles between the surface normal and the long molecular axes and the substituent axes, are denoted as γ, and θ. μ_z is the component of the molecular dipole moment along the surface normal calculated for the substituted backbones in the geometries they assume in the SAM; namely, in the calculation of μ_z, no depolarization effects are considered. β is the angle between the total molecular dipole moment and the surface normal. As there are two non-equivalent molecules in the unit cell, the average values for γ, θ, β, and μ_z are given.

Systems	ΔE_{HOPS} [eV]	IP_{SAM} [eV]	$\Delta\Phi$ [eV]	γ [°]	θ [°]	β [°]	μ_z [D]
S-**C1**-NH_2	−3.80	7.09	−1.86	11	42	75	0.33
S-**C1**-CN [a]	−3.96	10.21	1.02	7	64	51	−2.65
S-**C2**-NH_2	−0.86	3.57	−2.43	17	14	37	1.92
S-**C2**-CN	−0.93	8.83	2.62	12	15	14	−5.23
S-**C3**-NH_2	−0.43	2.87	−2.68	27	54	38	3.25
S-**C3**-CN [a]	−0.43	7.23	1.57	19	62	42	−4.52
S-**T1**-NH_2	−0.51	2.77	−2.86	7	18	33	2.08
S-**T1**-CN	−0.51	8.19	2.42	6	22	21	−5.29
S-**T2**-NH_2	−0.45	3.01	−2.58	20	35	43	1.94
S-**T2**-CN	−0.47	7.66	1.95	20	40	31	−4.62
S-**T3**-NH_2	−0.40	2.90	−2.63	23	36	40	2.53
S-**T3**-CN	−0.39	7.53	1.89	22	41	32	−5.10

[a] Internal-coordinate optimization of these systems leads to slow convergence near the local minimum. Therefore, based on the geometry pre-optimized with internal coordinates, another Cartesian-coordinate optimization was performed to reach the local minimum.

system (controlled by the metal); E_{vac}^{left} and E_{vac}^{right} are the vacuum levels at the left and right sides of the slab; IP_{SAM} is the ionization potential of the SAM; Φ_{Au} is the work function of Au(111), and $\Delta\Phi$ is the SAM-induced work-function modification. From the molecular density of states (MDOS, that is, the density of states projected onto the region of the SAM[30]) shown in the right panel of Figure 3, the position of the highest occupied π-states (HOPS) can be determined. For the sake of consistency, the highest fully delocalized state in **C1** is also referred to as HOPS although it is actually of σ-character (see Section 2.1).

The most relevant quantity for charge-carrier injection into the SAM is ΔE_{HOPS}, the energetic position of the HOPS relative to E_F. In principle, a similar reasoning holds also for the lowest unoccupied π-states (LUPS), which determine the electron-injection barriers. However, as DFT is known to poorly describe unoccupied molecular orbitals, we refrain from explicitly discussing the corresponding quantities in the present manuscript. The level alignment for all backbones with donor and acceptor substituents is summarized in Table 2. For each backbone, ΔE_{HOPS} is virtually independent of the substituent, whereas appreciable differences in IP_{SAM} are found between CN- and NH_2-substituted SAMs (calculated to be as high as 5.42 eV for **T1**). Remarkably, this behavior is observed in spite of the strongly varying backbone properties including *IP*s, HOMO energies, dipole moments, and, most notably, also polarizabilities and chemical hardness. In all systems investigated here, the substituents only affect the potential landscapes at the head-group side (and thus E_{vac}^{right}). They have no direct impact on the metal/SAM

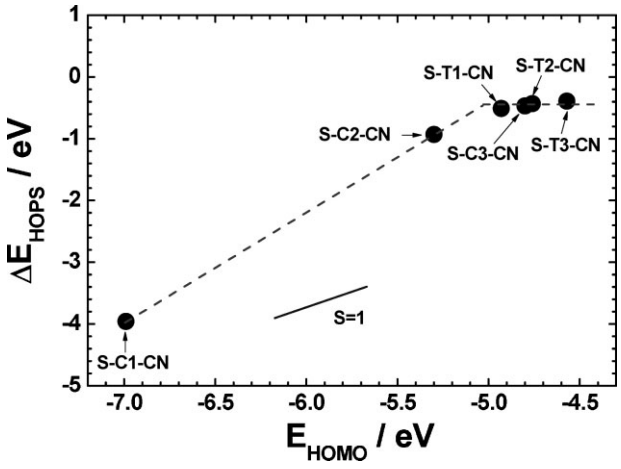

Figure 4. Energy difference between the highest occupied delocalized states in the SAM and the Fermi level, ΔE_{HOPS}, as a function of the energy of the highest occupied delocalized molecular orbital of the isolated backbone, E_{HOMO}. The dashed lines are a guide to the eye to better visualize the Fermi-level pinning. For comparison, a solid line with a slope of one is also shown.

interface in densely packed monolayers.[22] This somewhat counterintuitive finding thus refutes both chemically plausible strategies proposed in the Introduction and suggests that it is not a molecular property that is responsible for the effect. Instead, it must be a consequence of collective electrostatic effects in the monolayer, as pointed out by Natan et al., who argued that in a SAM represented by a densely packed 2D array of dipoles (located mostly on the head groups), the electric field emanating from this dipole layer decays on a length-scale shorter than the interdipole distance and also the length of the molecules (i.e., the thickness of the SAM).[44]

What does, however, have a significant impact on the level alignment is the chemical structure of the backbone itself (independent of any head-group substituent): As seen in Table 2, ΔE_{HOPS} is largest for the aliphatic backbone **C1**, intermediate for the aromatic system **C2**, and smallest for the non-aromatic conjugated systems (**C3**, **T1**, **T2**, and **T3**). A more systematic picture evolves when plotting ΔE_{HOPS} as a function of the HOMO energy of the isolated backbones (E_{HOMO} from Table 1). The results for the CN-substituted SAMs are shown in Figure 4; the plot for the $-NH_2$ substituents (not shown) looks virtually the same. One observes a steady decrease of ΔE_{HOPS} with decreasing E_{HOMO}. As the HOPS approaches E_F, the evolution levels off and the HOPS gets pinned approximately 0.3–0.4 eV below the metal Fermi level.[45] This can be rationalized by the following consideration: as soon as the onset of the HOPS crosses E_F (because of a small molecular *IP* of the backbone), electrons start being redistributed from the HOPS to the metal.[35] As the HOPS are delocalized over the entire backbone, a very small amount of charge transfer already gives rise to a sizable extra bond-dipole that keeps the HOPS peak below E_F. Consequently, only a small portion of the tail of the HOPS peak lies above the Fermi level.

For the design of SAMs in organic and molecular electronics these findings imply that, in addition to the docking group,[21,25] the choice of the molecular backbone is also a viable parameter for

tuning ΔE_{HOPS}. That is, varying the chemical structure of the backbone allows the tunnel barrier from electrodes through SAMs into an active organic material in plastic electronic devices to be adjusted and, furthermore, allows the current–voltage characteristics of single-molecule junctions to be modified.

A quantity that is affected by both the type of the backbone and the head-group substituent is IP_{SAM} (see Table 2). IP_{SAM} is related to the SAM-induced work-function change, $\Delta\Phi$, as well as to Φ_{Au} and the ΔE_{HOPS} via $\Delta\Phi = IP_{SAM} + \Delta E_{HOPS} - \Phi_{Au}$ (see Fig. 2). The very different dependence of IP_{SAM} and ΔE_{HOPS} on substitution and backbone hints towards a strong effect of the SAM chemical structure on $\Delta\Phi$, which will be analyzed in the following section.

3.2. Work-Function Modification

When trying to systematically link $\Delta\Phi$ to both the backbone properties and substituents, a complex situation evolves. One can expect $\Delta\Phi$ to depend on three interwoven factors:

i) The *magnitude* of the molecular dipole moments, μ: We recall that μ is given by the intrinsic dipole moments of the substituents plus the dipoles induced by the charge transfer between the backbones and the donor/acceptor head-group substituents; the latter is governed by the (local) polarizability of the backbone. The macroscopic quantity $\Delta\Phi$ is related to the microscopic molecular parameter μ through the Helmholtz equation, which states that $\Delta\Phi$ is proportional to μ per surface area A, namely, the area per molecule.

ii) The *orientation* of the individual molecular dipole moments relative to the surface normal: This is a crucial parameter as only the component of the molecular dipole moments perpendicular to the surface, $\mu_z = \mu \cdot \cos(\beta)$, enters the Helmholtz equation $\Delta\Phi = -e \cdot \mu_z/(\varepsilon_0 A)$. Here, β denotes the angle between μ and the surface normal, e is the elementary charge, and ε_0 the vacuum permittivity.

iii) *Depolarization effects*: In a 2D arrangement of polarizable dipoles (all out-of-plane dipole components aligned in parallel), the dipole moment of each molecule is reduced compared to that of one isolated molecule. Each dipole induces oppositely oriented dipoles in all neighbors. This gives rise to significant packing-induced charge rearrangements, which are located both on the substituent and throughout the backbone.[29] This results in a net depolarization in SAMs of dipolar molecules[26,27,44] and, thus, in a less pronounced work-function modification.[28] Naturally, the magnitude of this effect depends on the polarizability of the backbones. More precisely, again only the local polarizability in the vicinity of the substituent matters in densely packed SAMs (see point (i) in this discussion).[29]

The work-function modifications for all the investigated systems are given in Table 2 together with the orientations of the molecules in the SAM. The latter are specified by the angles between the surface normal and the long molecular axes (γ), the substituent axes (θ), and the dipole axes (β), which generally do not coincide with each other. The average angles for the two non-equivalent molecules in the unit cell are reported. To elucidate the correlation between the molecular dipole moment and the achieved work-function change,[46–48] $\Delta\Phi$ is plotted as a function of the absolute value of μ_{CN} and μ_{NH2} (taken from Table 1) in Figure 5 (solid black symbols). As expected, the CN-substitution results in a work-function increase, while NH_2-substitution leads to a decrease of Φ. The absolute magnitude of $\Delta\Phi$ is similar for both types of substitution, which might be unexpected at first glance considering the larger molecular dipole moments of the CN-substituted molecules (Table 1). It can, however, be explained by the contributions from the thiol docking groups (not considered when calculating the molecular dipole moments) and by the bond-dipoles resulting from the charge rearrangements at the metal/SAM interface upon S–Au bond formation and hydrogen removal.[22]

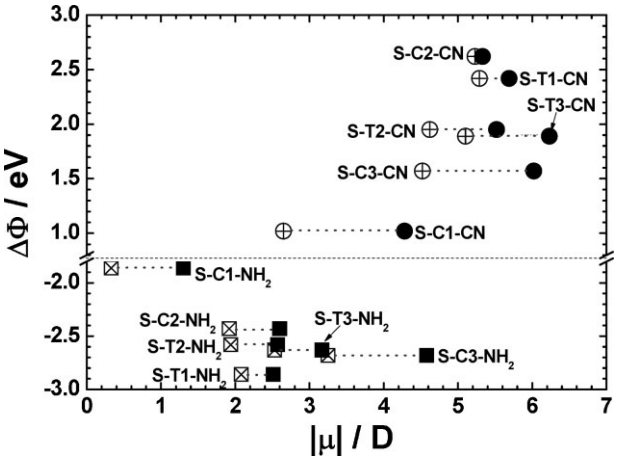

Figure 5. Dependence of the work-function modification, $\Delta\Phi$, on the molecular dipole moment, μ. Solid symbols denote $\Delta\Phi$ as a function of the total molecular dipole moments ($|\mu_{CN}|$ or $|\mu_{NH2}|$ from Table 1). Crossed symbols denote $\Delta\Phi$ as a function of μ_z, the (average) component of the molecular dipole moment perpendicular to the surface (see caption of Table 2). The dotted lines connect the two data points for each SAM. Note the break in the y axis.

What is even more surprising is the fact that there is hardly any correlation between the total molecular dipole moments (μ_{CN} and μ_{NH2}) and $\Delta\Phi$ (point (i) from above). Similarly, no clear trends are found when, for example, plotting $\Delta\Phi$ as a function of the energy of the molecular HOMO (i.e., in a plot analogous to Fig. 4 (not shown)). The correlation is somewhat improved when plotting the work-function modification as a function of only the perpendicular component, μ_z, of the molecular dipole (crossed symbols in Fig. 5). In this case, the orientation of the dipole moments is also considered (point (ii) from above). The largest relative differences between μ_{CN}/μ_{NH2} and the respective μ_z are found in the **C1**-based systems (Table 2), as one might already have expected from the fact that in these molecules the dipole axes deviate most strongly from the long molecular axes.

Remarkably, by far the clearest trend in the evolution of the work-function modification is found when plotting $\Delta\Phi$ as a function of the cosine of β, the angle between the molecular dipole moments and the surface normal (Fig. 6). The latter is calculated for isolated NH_2- or CN-substituted backbones in the same geometry as they normally adopt in the SAM. A strong correlation and a near-linear dependence of $\Delta\Phi$ on $\cos(\beta)$ is observed; the dashed lines in Figure 6 are linear fits to all the data points within

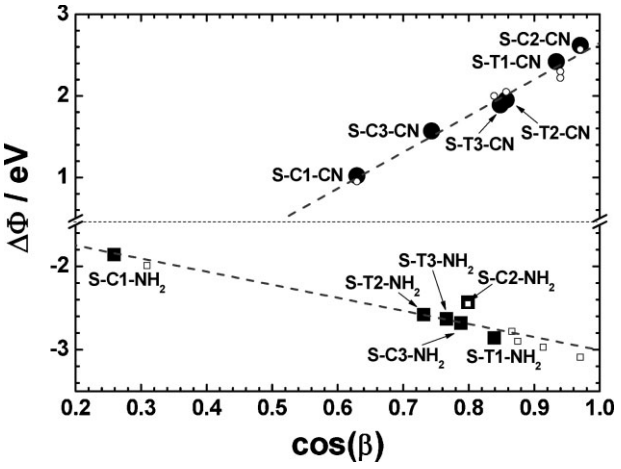

Figure 6. Dependence of the work-function modification, $\Delta\Phi$, on the cosine of β, the angle between the dipole axes of the individual molecules relative to the surface normal (see caption of Table 2); as there are two non-equivalent molecules in the unit cell, the average angle is shown. The large solid symbols are the data for the SAM structures obtained with internal-coordinate optimization. For comparison, data are also shown for SAM structures obtained with optimization in Cartesian coordinates (small open symbols); see text for details. The dashed lines are linear fits to the respective solid and open data points. Note the break in the *y* axis.

the same head group. This is insofar unexpected as the actual magnitude of the molecular dipole moments is not considered in this figure. This indicates that the chemical nature of the backbone has no direct impact on $\Delta\Phi$ and that the orientation of the molecular dipole moment with respect to the surface normal is, in fact, the dominant parameter for the work-function modification. To ensure that this observation is not an artifact of some sort, we calculated $\Delta\Phi$ for a second set of molecular orientations, namely the ones obtained from geometry optimizations in Cartesian coordinates. As discussed in Section 2.2, they do not correspond to actual minimum structures with respect to the molecular tilt angle but, as the geometries are otherwise converged and very likely accessible at room temperature, this does not compromise the appropriateness of this test. The resulting values for $\Delta\Phi$ ($\cos(\beta)$) are shown as small open circles in Figure 6; reassuringly, they follow the same linear evolution.

To understand how variations of the molecular dipole moments across different backbones can be of only minor significance, one has to remember the origin of those variations and one also needs to consider the last of the above-mentioned factors, depolarization: we recall that the molecular dipole moments are a combination of the intrinsic dipole moments of the substituent groups and the induced dipoles arising from charge transfer between the substituents and backbones. The latter increases with increasing (local) backbone polarizability. However, depolarization effects also increase with backbone polarizability; as a result, the effective dipole moment per molecule in the SAM is largely reduced. The data shown in Figure 6 then imply that the component of the molecular dipole, which is related to backbone/head-group charge transfer, and the ''counter-dipole'', induced by the electric field generated by all neighboring dipolar molecules (as a result of the substituent *and* induced dipoles), largely cancel each other out in the systems studied here (at least at full coverage, see below). We note that, furthermore, two additional effects are superimposed on the mechanism just described which can, in part, be held responsible for the remaining scatter in $\Delta\Phi$. The bond-dipole at the metal/SAM interface related to charge rearrangements upon hydrogen cleavage and S−Au bond formation[21,22] exhibits a certain tilt-angle dependence[43,49] and the dipole arising from the pinning of the HOPS (Section 3.1) has an impact on $\Delta\Phi$ as well.

For the design of SAMs that promote carrier injection into organic electronic devices these findings underline that control over the orientation of the dipolar substituents is vitally important for predictably tuning the SAM-induced work-function modification; we emphasize that this orientation, albeit related to the backbone structure, is not the same parameter as the backbone orientation itself. Once structural control is achieved, varying the dipole orientation by choice of backbone opens up the possibility of also optimizing the substituents with regard to parameters other than their dipole moment, for instance, hydrophobicity/-philicity or (bio)chemical reactivity. However, it has to be borne in mind that the backbone orientation (γ) and, thus, also the dipole orientation (β) are very soft structural degrees of freedom. Therefore, one can expect significant dynamic fluctuations of γ, β, and, consequently, also $\Delta\Phi$ at finite temperatures.

3.3. The Impact of Coverage

To better illustrate the impact of the backbone on depolarization effects and, furthermore, to assess the consequence of disorder, imperfections, and/or reduced coverage (often encountered in experiments), we consider the packing-density dependence of the work-function modification in the following. To that end, as a simplified model case, molecules are successively removed from a large supercell[50] in analogy to the procedure previously described in the literature.[28] There, it has been shown that depolarization indeed leads to a pronounced packing-density dependence of both the level alignment and work-function modification in biphenyl-based SAMs (**C2**).

Here, we extend that study to different backbones (Fig. 1) by evaluating $\Delta\Phi$ for the SAM-covered Au surfaces at coverages between $\tau = 1/16$ and $\tau = 1$, with 1 referring to densely packed layers. The quantity $\Delta\Phi(\tau)/\tau$ is an approximate measure for how large the work-function modification would be at full coverage, if there was only the amount of depolarization present that one encounters at coverage τ. Assuming close to zero depolarization at $\tau = 1/16$,[29] the value for $\Delta\Phi$ (1/16)/(1/16) serves as an estimate of how large the work-function modification could become in the absence of depolarization.

The evolution of $\Delta\Phi(\tau)/\tau$ normalized to the values calculated at full coverage (i.e., the values reported in Table 2) is shown in Figure 7 for the -NH_2 substituent. The significance of depolarization effects becomes obvious. Already for the ''reference system'' **C2**, the achievable work-function modification at full coverage would be a factor of around 3.4 larger in the absence of depolarization.[51] For the more polarizable backbones the effect is even more pronounced with depolarization being strongest for **T3**. There, the work-function modification at full coverage would be larger by a factor of about 5.2 in the absence of depolarization.

These results confirm the importance of depolarization effects on the achievable work-function modification in dipolar SAMs

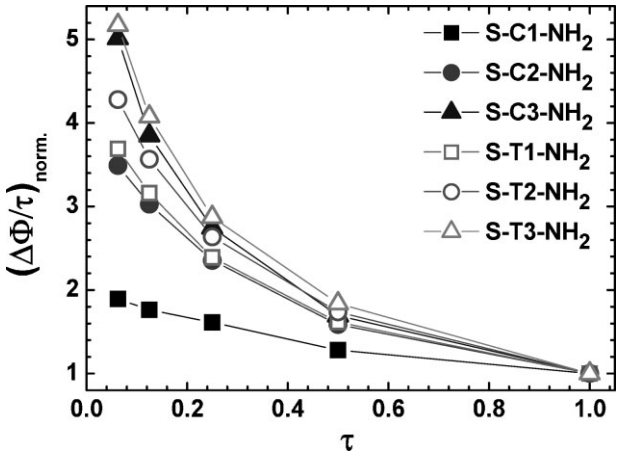

Figure 7. Effective depolarization for the NH_2-substituted SAMs as a function of coverage. The quantity $(\Delta\Phi/\tau)_{norm.}$ is defined as the work-function modification at a particular coverage divided by that coverage and normalized to $\Delta\Phi$ at full coverage ($\tau = 1$), that is, $\Delta\Phi(\tau)/\tau/\Delta\Phi(1)$. The plot illustrates how much larger the work-function modification would be when gradually ''turning off'' depolarization effects.

with backbones of varying polarizability. Furthermore, they illustrate the sizable impact of static disorder, that is, deviations from the ideally ordered, densely packed SAM structure, which are likely to appear in addition to the dynamic fluctuation of $\Delta\Phi$ discussed before.

4. Conclusions

We have presented a comprehensive first-principles study on SAMs of organic thiols on Au(111) surfaces. In particular, we have elucidated the role of the backbone polarizability on the alignment of the SAM states with the metal Fermi level, the effect of donor/acceptor head-group substitutions, and the SAM-induced modification of the metal work function. For densely packed SAMs, we have found that the electron-donating or -withdrawing character of the head-group substitutions has no impact on the level alignment, regardless of backbone properties. Different HOMO positions resulting from the nature of the backbone, however, do significantly affect the level alignment until pinning of the Fermi level close to the highest occupied delocalized states is observed for backbones characterized by small ionization potentials.

For all backbones, an increase of the work function for CN head-group substitutions and a decrease for NH_2-substitutions was consistently observed. Surprisingly, the orientation of the molecular dipole moments (largely localized on these head groups) and not the magnitude of the backbone-dependent, induced molecular dipole moments is identified as the dominant factor for the work-function modification when comparing different backbones. This is attributed to the canceling of two factors, namely the larger substituent-induced dipole moment in more polarizable backbones and the concurrent increase of depolarization in densely packed SAMs.

As the orientation of the molecules relative to the surface normal represents a rather soft degree of freedom, significant dynamic fluctuations of the work function can be expected at finite temperature. Moreover, deviations from the ideal SAM structure are shown to affect the work function in a nontrivial manner because of the complex coverage dependence of the involved depolarization phenomena.

For molecular design, our findings underline that the chemical structure of the backbone is an important parameter determining the tunnel barriers through SAMs. Moreover, through the interrelation between backbone structure and dipole-moment orientation, variation of the backbone allows for tuning the charge-injection barriers from electrodes into the active organic materials in plastic electronic devices.

5. Experimental

All calculations presented here are based on DFT. For calculations of monolayers on Au(111), the Vienna ab-initio Simulation Package (VASP) version 4.6 [52–54] with a plane-wave basis set at an energy cutoff of 20 Ryd was used. The PW91 exchange-correlation functional [55] was used together with the projector augmented-wave method (PAW) to describe valence–core interactions [56,57]. A Monkhorst–Pack [58] k-point grid of $(8 \times 5 \times 1)$ was applied in full coverage for the self-consistent field calculations in combination with a second-order Methfessel–Paxton occupation scheme for the density of states (DOS) with a broadening of 0.2 eV [59]. All calculations were carried out in a non-spin-polarized manner. For reduced coverage calculations, we followed the process used in a previous study, where larger surface supercells are considered and molecules are successively removed from those supercells [28]. The geometries of those supercells at reduced coverage are not re-optimized as then the effects of depolarization would be superseded by the impact of increased tilt angles at low coverage.

In the geometry optimizations, all atoms of the molecules and the top two Au layers were fully optimized until the remaining forces were less than 0.01 eV $Å^{-1}$; the bottom three Au layers were kept fixed at their bulk positions. When performing geometry optimizations in Cartesian coordinates using the damped molecular dynamics scheme implemented in VASP, calculations became trapped at saddle points or local minima (data given in the Supporting Information). In contrast, optimization in internal coordinates is know to be particularly suited for identifying the minimum of the potential surface with respect to soft degrees of freedom such as the tilt angle of the SAM molecules. Consequently, as this angle proved to be a crucial parameter for a reliable description of the SAM-induced work-function modifications, a recently developed optimization scheme based on internal coordinates was used [41]. As discussed in the main text and exemplified in the Supporting Information, several structures at local minima can also be identified as having very similar total energies. As these minima are characterized for instance by different orientations of the slightly pyramidal -NH_2 groups (and thus differing local dipoles), they are characterized by different values for $\Delta\Phi$. Considering these complications (i.e., the large number of energetically close-lying local minima), one cannot be absolutely sure that, in spite of our considerable efforts, we always succeeded in identifying the global minimum structures. Moreover, in view of the minute dependence of the total energy on the tilt angle, minor variations in the applied methodology could already change that parameter noticeably. None of these aspects affect the fundamental conclusions drawn, but to ensure full reproducibility of our results, we have included the coordinate files for all those minimum-energy conformations in the Supporting Information for which the data described in the main text were obtained.

To identify the HOPS, that is, the highest occupied molecular states in the SAM that are fully delocalized along the backbone, it must be borne in mind that, because of lateral electronic interaction between the molecules in the SAM, weakly dispersing 2D bands are formed from the orbitals of the free molecules. Together with metal/molecule interactions, this gives rise

to a broadening of the corresponding peaks in the density of states of the entire Au-slab/SAM system projected onto the molecular region (MDOS). Analyzing the local DOS (LDOS) integrated in an energy window around the highest-energy MDOS peaks allows confirmation of the delocalized nature of the corresponding states (see Supporting Information). Following this procedure, the HOPS energy was determined as the position of the MDOS peak closest to E_F for all systems apart from **C1**, where the third-closest peak was found to be fully delocalized along the backbone (see Supporting Information). Additionally, the influence of the broadening factor in the Methfessel–Paxton occupation scheme was tested (see Supporting Information). Its impact on the determined HOPS position was found to be in the range of 0.05 eV and, therefore, only of minor importance for level alignment and pinning.

The properties of isolated molecules were calculated using the Gaussian 03 Rev. E.01 program suit [60]. The PW91/PW91 exchange-correlation functional (aiming at consistency with the band-structure calculations) was employed in conjunction with a 6-31G** basis set. The molecular geometries were optimized with all backbones forced to be planar. This is reasonable insofar as all backbones adopt a planar structure in the SAM, even if some of the molecules (e.g., the substituted biphenyls) are twisted in the gas phase. Test calculations using the B3LYP functional and including diffuse basis functions yielded similar trends.

Acknowledgements

Support from the Ministry of Science and Technology of China through the 973 program (Grant Nos. 2006CB806200, 2006CB932100, and 2009CB623600) is greatly acknowledged. The work in Graz is supported by the FWF through project P20972-N20. G. Heimel acknowledges financial support by the DFG through Sfb448 ''Mesoscopically Organized Composites''. Supporting Information is available online from Wiley InterScience or from the authors.

Received: June 26, 2009
Published online: November 2, 2009

[1] G. S. Tulevski, C. Nuckolls, A. Afzali, T. O. Graham, C. R. Kagan, *Appl. Phys. Lett.* **2006**, *89*, 183101.
[2] N. Koch, *Chem. Phys. Chem.* **2007**, *8*, 1438.
[3] D. Natali, L. Fumagalli, M. Sampietro, *J. Appl. Phys.* **2007**, *101*, 014501.
[4] J. Zaumseil, H. Sirringhaus, *Chem. Rev.* **2007**, *107*, 1296.
[5] B. Stadlober, U. Haas, H. Gold, A. Haase, G. Jakopic, G. Leising, N. Koch, S. Rentenberger, E. Zojer, *Adv. Funct. Mater.* **2007**, *17*, 2687.
[6] C. Vanoni, S. Tsujino, T. A. Jung, *Appl. Phys. Lett.* **2007**, *90*, 193119.
[7] F. Fujimori, K. Shigeto, T. Hamano, T. Minari, T. Miyadera, K. Tsukagoshi, Y. Aoyagi, *Appl. Phys. Lett.* **2007**, *90*, 193507.
[8] I. H. Campbell, J. D. Kress, R. L. Martin, D. L. Smith, N. N. Barashkov, J. P. Ferraris, *Appl. Phys. Lett.* **1997**, *71*, 3528.
[9] C. D. Zangmeister, L. B. Picraux, R. D. van Zee, Y. Yao, J. M. Tour, *Chem. Phys. Lett.* **2007**, *442*, 390.
[10] K. Demirkan, A. Mathew, C. Weiland, Y. Yao, A. M. Rawlett, J. M. Tour, R. L. Opila, *J. Chem. Phys.* **2008**, *128*, 074705.
[11] P. Marmont, N. Battaglini, P. Lang, G. Horowitz, J. Hwang, A. Kahn, C. Amato, P. Calas, *Org. Electron.* **2008**, *9*, 419.
[12] C. Bock, D. V. Pham, U. Kunze, D. Käfer, G. Witte, C. Wöll, *J. Appl. Phys.* **2006**, *100*, 114517.
[13] C. H. Ahn, A. Bhattacharya, M. D. Ventra, J. N. Eckstein, C. D. Frisbie, M. E. Gershenson, A. M. Goldman, I. H. Inoue, J. Mannhart, A. J. Millis, A. F. Morpurgo, D. Natelson, J.-M. Triscone, *Rev. Mod. Phys.* **2006**, *78*, 1185.
[14] L. A. Bumm, J. J. Arnold, M. T. Cygan, T. D. Dunbar, T. P. Burgin, L. Jones, II, D. L. Allara, J. M. Tour, P. S. Weiss, *Science* **1996**, *271*, 1705.
[15] J. Chen, M. A. Reed, A. M. Rawlett, J. M. Tour, *Science* **1999**, *286*, 1550.
[16] J. G. Kushmerick, D. B. Holt, J. C. Yang, J. Naciri, M. H. Moore, R. Shashidhar, *Phys. Rev. Lett.* **2002**, *89*, 086802.
[17] D. J. Wold, C. D. Frisbie, *J. Am. Chem. Soc.* **2001**, *123*, 5549.
[18] C. D. Zangmeister, S. W. Robey, R. D. van Zee, Y. Yao, J. M. Tour, *J. Phys. Chem. B* **2004**, *108*, 16187.
[19] A. Nitzan, M. A. Ratner, *Science* **2003**, *300*, 1384.
[20] Y. Q. Xue, M. A. Ratner, *Phys. Rev. B* **2003**, *68*, 115407.
[21] G. Heimel, L. Romaner, E. Zojer, J.-L. Brédas, *Nano Lett.* **2007**, *7*, 932.
[22] G. Heimel, L. Romaner, J.-L. Brédas, *Phys. Rev. Lett.* **2006**, *96*, 196806.
[23] G. M. Rangger, L. Romaner, G. Heimel, E. Zojer, *Surf. Interface Anal.* **2008**, *40*, 371.
[24] The 4′ position of the biphenyl-thiolate is the ''easily accessible'' end that points away from the metal.
[25] G. Heimel, L. Romaner, E. Zojer, J. L. Brédas, *Acc. Chem. Res.* **2008**, *41*, 721.
[26] A. Natan, Y. Zidon, Y. Shapira, L. Kronik, *Phys. Rev. B* **2006**, *73*, 193310.
[27] D. Cornil, Y. Olivier, V. Geskin, J. Cornil, *Adv. Funct. Mater.* **2007**, *17*, 1143.
[28] L. Romaner, G. Heimel, E. Zojer, *Phys. Rev. B* **2008**, *77*, 045113.
[29] L. Romaner, G. Heimel, C. Ambrosch-Draxl, E. Zojer, *Adv. Funct. Mater.* **2008**, *18*, 3999.
[30] G. Heimel, L. Romaner, J.-L. Brédas, E. Zojer, *Surf. Sci.* **2006**, *600*, 4548.
[31] G. Heimel, L. Romaner, E. Zojer, J. L. Brédas, *Proc. SPIE* **2008**, *6999*, 699 919.
[32] Q. Sun, A. Selloni, *J. Phys. Chem. A* **2006**, *110*, 11396.
[33] Q. Sun, A. Selloni, G. Scoles, *J. Phys. Chem. B* **2006**, *110*, 3493.
[34] A. Kahn, N. Koch, W. Y. Gao, *J. Polym. Sci, Part B: Polym. Phys.* **2003**, *41*, 2529.
[35] S. Braun, W. R. Salaneck, M. Fahlman, *Adv. Mater.* **2009**, *21*, 1450.
[36] R. G. Pearson, *Science* **1966**, *151*, 172.
[37] R. G. Parr, R. G. Pearson, *J. Am. Chem. Soc.* **1983**, *105*, 7512.
[38] N. Camillone, III, C. E. D. Chidsey, G. Liu, G. Scoles, *J. Chem. Phys.* **1993**, *98*, 3503.
[39] G. E. Poirier, M. J. Tarlov, *Langmuir* **1994**, *10*, 2853.
[40] W. Azzam, C. Fuxen, A. Birkner, H. Rong, M. Buck, C. Wöll, *Langmuir* **2003**, *19*, 4958.
[41] T. Bučko, J. Hafner, J. G. Ángyán, *J. Chem. Phys.* **2005**, *122*, 124508.
[42] When comparing optimizations in Cartesian and internal coordinates, we find that for geometries that are sometimes only a few hundredth of an electron-volt higher in energy but are characterized by a significantly different twist angle, variations of the SAM-induced work-function modifications of up to 1.60 eV can occur (with the largest effect observed for S-**C1**-NH_2).
[43] F. Rissner, T. Bučko, A. M. Track, G. M. Rangger, L. J. Wang, Z. Shuai, E. Zojer, unpublished.
[44] A. Natan, L. Kronik, H. Haick, R. T. Tung, *Adv. Mater.* **2007**, *19*, 4103.
[45] The exact energy at which the HOPS becomes pinned is somewhat influenced by the applied broadening factors in the Methfessel–Paxton occupation scheme. The error of HOPS pinning position is, however, expected to be within 0.05 eV (see test calculations described in the Supporting Information).
[46] R. W. Zehner, B. F. Parsons, R. P. Huang, L. R. Sita, *Langmuir* **1999**, *15*, 1121.
[47] D. M. Alloway, M. Hofmann, D. L. Smith, N. E. Gruhn, A. L. Graham, J. R. Colorado, Jr, V. H. Wysocki, T. R. Lee, P. A. Lee, N. R. Armstrong, *J. Phys. Chem. B* **2003**, *107*, 11690.
[48] M. Malicki, Z. Guan, S. D. Ha, G. Heimel, S. Barlow, M. Rumi, A. Kahn, S. R. Marder, *Langmuir* **2009**, *25*, 7967.
[49] G. Heimel, L. Romaner, J.-L. Brédas, E. Zojer, *Langmuir* **2008**, *24*, 474.
[50] In those calculations, the geometries at reduced coverage are not re-optimized because this i) would overstretch the limits of present computational capacities and ii) is not useful for the points discussed here as the main change in geometry would be a severe increase of the tilt angle.
[51] This factor is 4.0 in the literature [23] as Cartesian-coordinate optimized geometries have been used. As the internal-coordinate optimization mainly affects the tilt angle, this influences the depolarization strength.

[52] G. Kresse, J. Hafner, *Phys. Rev. B* **1993**, *47*, 558.
[53] G. Kresse, J. Hafner, *Phys. Rev. B* **1994**, *49*, 14251.
[54] G. Kresse, J. Furthmüller, *Phys. Rev. B* **1996**, *54*, 11169.
[55] S. Tsuzuki, H. P. Lüthi, *J. Chem. Phys.* **2001**, *114*, 3949.
[56] P. E. Blöchl, *Phys. Rev. B* **1994**, *50*, 17953.
[57] G. Kresse, D. Joubert, *Phys. Rev. B* **1999**, *59*, 1758.
[58] H. J. Monkhorst, J. D. Pack, *Phys. Rev. B* **1976**, *13*, 5188.
[59] M. Methfessel, A. T. Paxton, *Phys. Rev. B* **1989**, *40*, 3616.
[60] M. J. Frisch, G. W. Trucks, H. B. Schlegel, G. E. Scuseria, M. A. Robb, J. R. Cheeseman, J. A. Montgomery, Jr, T. Vreven, K. N. Kudin, J. C. Burant, J. M. Millam, S. S. Iyengar, J. Tomasi, V. Barone, B. Mennucci, M. Cossi, G. Scalmani, N. Rega, G. A. Petersson, H. Nakatsuji, M. Hada, M. Ehara, K. Toyota, R. Fukuda, J. Hasegawa, M. Ishida, T. Nakajima, Y. Honda, O. Kitao, H. Nakai, M. Klene, X. Li, J. E. Knox, H. P. Hratchian, J. B. Cross, V. Bakken, C. Adamo, J. Jaramillo, R. Gomperts, R. E. Stratmann, O. Yazyev, A. J. Austin, R. Cammi, C. Pomelli, J. W. Ochterski, P. Y. Ayala, K. Morokuma, G. A. Voth, P. Salvador, J. J. Dannenberg, V. G. Zakrzewski, S. Dapprich, A. D. Daniels, M. C. Strain, O. Farkas, D. K. Malick, A. D. Rabuck, K. Raghavachari, J. B. Foresman, J. V. Ortiz, Q. Cui, A. G. Baboul, S. Clifford, J. Cioslowski, B. B. Stefanov, G. Liu, A. Liashenko, P. Piskorz, I. Komaromi, R. L. Martin, D. J. Fox, T. Keith, M. A. Al-Laham, C. Y. Peng, A. Nanayakkara, M. Challacombe, P. M. W. Gill, B. Johnson, W. Chen, M. W. Wong, C. Gonzalez, J. A. Pople, Gaussian 03, Revision A.1, Gaussian, Inc, Wallingford, CT **2004**.